Journal of Materials Chemistry B

RSC Publishing

PAPER

Amphiphilic silver-delaminated clay nanohybrids and their composites with polyurethane: physico-chemical and biological evaluations†

Cite this: *J. Mater. Chem. B*, 2013, **1**, 2178

Ting-Yen Chi,[a] Hsi-Yi Yeh,[a] Jiang-Jen Lin,[a] U-Ser Jeng[b] and Shan-hui Hsu*[a]

Received 25th January 2013
Accepted 26th February 2013

DOI: 10.1039/c3tb20113a

www.rsc.org/MaterialsB

Silver nanoparticles (AgNPs) exhibit size-dependent bactericidal activity. They are, however, subject to aggregation when added to most hydrophobic polymers. In this study, a surfactant-modified delaminated clay (surfactant-capped nanosilicate platelets, or "NSQ") was employed to be a nanocarrier for AgNPs. The nanohybrid of AgNPs and NSQ ("AgNP/NSQ") in aqueous solution showed remarkable bactericidal effect as well as negligible cytotoxicity and immune response at a concentration of 10 ppm. Poly(carbonate)urethane (PCU) with different hard/soft segment ratios was synthesized and used in the preparation of the nanocomposites, PCU-AgNP/NSQ. Based on TEM observation, AgNP/NSQ was well dispersed in the resulting nanocomposites. The reinforcing effects of AgNP/NSQ in nanocomposites were distinct for PCU with different hard/soft segment ratios. The phase-separated structure of PCU-AgNP/NSQ nanocomposites was investigated by small-angle X-ray scattering (SAXS). PCU-AgNP/NSQ containing 75 ppm of Ag demonstrated superior microbiostatic effect, as well as better biodurability and lower foreign body reaction than the commercial Pellethane 2363-80A.

Introduction

Silver nanoparticles (AgNPs) show remarkable bactericidal activity. The small size and good dispersion state of AgNPs are crucial for their antibacterial efficacy.[1,2] AgNPs also exhibit cytotoxic and genotoxic effects in mammalian cells. They may accumulate in the mitochondria and nuclei of human lung fibroblasts or glioblastoma cells, leading to excessive production of reactive oxygen species (ROS) and cellular damage.[3] Small AgNPs were found to up-regulate the expressions of proinflammatory genes and induce the immune response of macrophages.[4,5] The antimicrobial activity as well as cytotoxicity was more pronounced for smaller AgNPs.[4]

Silicate clays have potential biomedical applications including wound healing.[6] To reduce particle aggregation and prevent AgNPs from entering the cells, clay was employed as a carrier for AgNPs. The nanohybrid of silver and clay successfully rendered non-aggregated AgNPs.[7] The compact layered structures of montmorillonite clay may be completely delaminated by a novel process and give individual thin platelets of silicate of $80 \times 80 \times 1$ nm dimension, the so called nanosilicate platelets (NSP).[8] NSP can be stably suspended in water[8] and undergo self-assembly at certain conditions.[9] The high aspect ratio and strong charge density of NSP might lead to trapping force and inhibition of the bacterial growth,[10] without causing significant cytotoxicity or genotoxicity.[11] NSP can serve as an excellent carrier for AgNPs to prevent their aggregation.[12] Compared with the stabilizer-capped AgNPs, the nanohybrid of AgNPs and NSP ("AgNP/NSP") may have better surface activities because AgNPs are not capped. The relatively bulky size of NSP may prevent the nanohybrid from entering cells while maintaining the functionality of small AgNPs.

Polyurethane (PU) is formed by the reaction of isocyanates with a chain extender (hard segment) and macrodiol (soft segment). The incompatibility between the two segments of PU results in microphase separation. The domains from aggregation of hard segments are dispersed in the matrix of the soft segment, leading to elasticity.[13,14] The physicochemical properties of PU can be regulated by changing its chemical structure including the length of the soft segment or by grafting with the other polymers.[15,16] The proper mechanical properties, chemical stability, thermoprocessibility[17,18] as well as the excellent antithrombotic property and biocompatibility make PU popular biomaterials.[19] The microphase-separated morphology of PU may influence the cellular response, blood compatibility, and immune reaction.[20–22] Compared with the polyester- or polyether-based PU, poly(carbonate)urethane (abbreviated "PCU") is more biodurable with better stabilities *in vitro*[23] and biocompatibility *in vivo*.[24] PU itself does not resist bacterial adhesion and often requires antibacterial treatment to prevent infections.

[a]*Institute of Polymer Science and Engineering, National Taiwan University, Taipei, 10617, Taiwan, R.O.C. E-mail: shhsu@ntu.edu.tw; Fax: +886 2 33665237; Tel: +886 2 33665313*

[b]*National Synchrotron Radiation Research Center, Hsinchu, 30076, Taiwan, R.O.C.*

† Electronic supplementary information (ESI) available: The cytotoxicity of the AgNP/NSQ nanohybrid, the expression of proinflammatory genes, attachment and proliferation of ECs on PCU and the data of macrophages on PCU or the nanocomposites. See DOI: 10.1039/c3tb20113a

Nanomaterials such as gold,[25] silica,[26] or organoclay[27] when loaded in a PU polymer may modify its phase separation and the surface properties. Making nanocomposites from AgNP/NSP may be potentially effective in enhancing the antimicrobial ability of PU-based materials. However, AgNP/NSP is dispersible in water but not in a hydrophobic polymer matrix. Surfactant-modification can help generate NSP that are dispersible in both water and polymers.[28,29] The amphiphilic nanohybrid of silver and surfactant-modified NSP ("AgNP/NSQ") may therefore be a good candidate of an antibacterial nanofiller for PU. In this study, we prepared the amphiphilic nanohybrid of AgNP/NSQ and evaluated the cytotoxicity, immune response, and antibacterial efficacy *vs.* AgNP/NSP. We then synthesized and characterized novel PCU as well as PCU-AgNP/NSQ nanocomposites. Small-angle X-ray scattering (SAXS) was used to analyze the phase-separated structure of PCU-AgNP/NSQ. Results of the antimicrobial activity, *in vitro* cytotoxicity, and *in vivo* biocompatibility suggested the success of this approach in establishing an antimicrobial and biodurable PU formulation.

Materials and methods

Preparation of AgNP/NSQ nanohybrid

NSP were prepared as previously described.[8] The amphiphilic surfactant-modified NSP ("NSQ") were further prepared from NSP using Sinopol 1830, a polyethylene oxide (PEO)-based surfactant. Sinopol was stirred in water for 20 min in a round-bottomed flask to which was added a 3 wt% NSP suspension. The mixture was agitated for 60 min, collected and freeze-dried. To prepare AgNP/NSQ, 30 g of 1 wt% NSQ water suspension was mixed with 3.5 g of 1 wt% silver nitrate aqueous solution in another round-bottomed flask. After stirring for 10 min, 0.5 g of 10 wt% diethanolamine aqueous solution was added and further stirred for 10 min. The reaction ran for 4 h at 50 °C and the products were collected and freeze-dried. The theoretical weight ratio of AgNPs to NSQ in the hybrid was 7/93. The steps for preparation of AgNP/NSQ nanohybrid are illustrated in Scheme 1. On the other hand, the hydrophilic AgNP/NSP nanohybrid was prepared as described.[12]

The organic fraction of NSQ was measured by a thermogravimetric analyzer (TGA, Perkin Elmer 7, Perkin Elmer, USA), with a heating rate of 10 °C per min from 100 to 750 °C. The silver content of AgNP/NSQ was measured by an atomic absorption spectrometer (AA, iCE-3000, Thermo, USA). To measure the possible contamination of unreacted silver ion or free (unattached) AgNPs in the final product of AgNP/NSQ, 0.1 wt% AgNP/NSQ aqueous solution was added (3 mL) in a centrifugal filter device (Millipore, USA) and centrifuged at 7500 rpm for 30 min. The filtrate was collected and diluted with double deionized water (DDW) or 0.5 N nitric acid. The concentrations of silver ion (diluted with DDW) and total silver (diluted with nitric acid) were analyzed by AA.

To determine the size and size-distribution of AgNPs immobilized on NSQ, AgNP/NSQ at a concentration of 100 ppm was cast on copper grids and examined by transmission electron microscopy (TEM, TEM-1230, JEOL, Japan). The TEM image was analyzed by Image-J software. The hydrodynamic diameter and zeta potential of AgNP/NSQ, AgNP/NSP, NSQ, NSP, and physically manufactured AgNPs (Gold Nano Tech. Taiwan) were measured based on dynamic light scattering using a particle analyzer (Delsa™Nano, Beckman Coulter, USA).

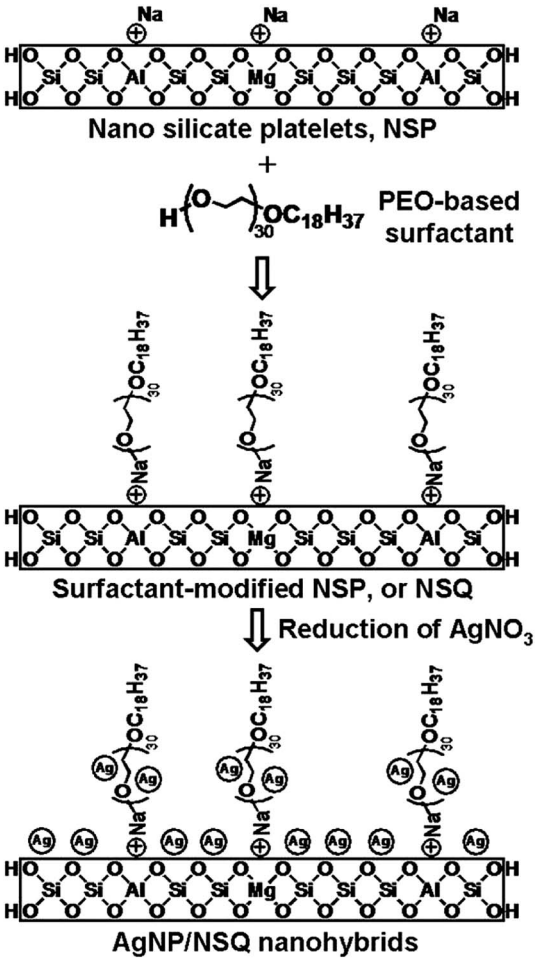

Scheme 1 Compositions of exfoliated clay NSP, surfactant-modified NSP (NSQ), and AgNP/NSQ nanohybrid.

Synthesis of PCU and preparation of nanocomposites with AgNP/NSQ

Poly(pentyl, hexyl)carbonate diol (PC diol, M_w = 2000, T-5652, Asahi-Kasei, Japan) was dried and degassed at 80 °C under vacuum for 4 h. 4,4′-Diphenylmethylene diisocyanate (MDI, Bayer, Germany) was placed at 60 °C for 24 h for collection of the pure liquid, which was used for synthesis. *N*,*N*-Dimethylacetamide (DMAc, TEDIA, USA) and 2-butene-1,4-diol (Sigma, USA) were dried by molecular sieves before use. To synthesize PCU, MDI was added to PC diol and reacted at 60 °C for 4 h. The solvent, DMAc, was added and 2-butene-1,4-diol was then dropped into the solution as a chain extender. Chain extension was performed at 70 °C for about 15.5 h when the amount of NCO reached the theoretical value determined by the dibutylamine titration. The polymer solution was then dropped into methanol to obtain granules. The granules were collected and dried at 60 °C under vacuum. Five types of PCU with different

stoichiometric ratios (MDI/PC diol/2-butene-1,4-diol = 2 : 1 : 1, 3 : 2 : 1, 4 : 3 : 1, 5 : 4 : 1, and 6 : 5 : 1) were synthesized. The molecular weight and polydispersity were measured by gel permeation chromatography (GPC, Waters Apparatus, USA).

To prepare nanocomposites, dried PCU granules were added to AgNP/NSQ in DMAc at different ratios and stirred for 24 h. Thin films (~0.02 mm) were cast on a 15 mm coverslip glass. Thicker films (~0.2 mm) were cast in Teflon dishes. All films were dried at 60 °C for 72 h and further dried under vacuum at 60 °C for 48 h. The final nanocomposites ("PCU-AgNP/NSQ") contained 227–1136 ppm of AgNP/NSQ, equivalent to 15–75 ppm of AgNPs. Pellethane (2363-80A; Upjohn, USA), a commercial biomedical grade PU, was used as the control.

Cytotoxicity, immune response and antibacterial activity of AgNP/NSQ nanohybrid

A mouse skin fibroblast cell line (L929) and a human hepatocarcinoma cell line (HepG2) were used for the cytotoxicity tests. The culture media used were low glucose Dulbecco's Modified Eagle's Medium (DMEM) (Gibco, USA) for L929 and minimum essential medium (MEM) (Gibco, USA) for HepG2. Both media contained 1% penicillin–streptomycin–amphotericin (PSA, Gibco, USA), 10% fetal bovine serum (FBS, Gibco, USA), and 1.7 g L^{-1} sodium bicarbonate. Cells were seeded in 24-well tissue culture plates at a density of 5×10^4 cells per well. After 24 h, the medium was removed, replaced by 0.1 mL tested sample (suspension of AgNP/NSQ, NSQ, AgNP/NSP, NSP, AgNPs, or silver nitrate) and 0.9 mL medium, and incubated for another 24 h. Normal culture medium (blank) served as the negative control and the medium containing 5% dimethyl sulfoxide (DMSO, Sigma, USA) served as the positive control. The cytotoxicity was evaluated by the 3-(4,5-dimethyl-thiazol-2-yl)-2,5-diphenyltetrazolium bromide (MTT) assay after exposure for 24 h. The absorbance was measured at 550 nm using a microplate reader and normalized to the negative control to obtain cell viability.

To evaluate the mitochondrial activity of HepG2 exposed to AgNP/NSQ, cells were seeded in an XF24 cell culture plate (Seahorse Bioscience, USA) with a density of 2×10^4 cells per well. After 24 h, the medium was removed and replaced by 0.675 mL medium containing 2% FBS. The culture plate was placed in the extracellular flux analyzer (XF extracellular flux analyzer, Seahorse Bioscience, USA). After reaching the equilibrium state, 75 μL of the sample solution (10×) was injected to the plate and the *in situ* oxygen consumption rate (OCR) and extracellular acidification rate (ECAR) were measured. The exposure endured for 85 min.

The intracellular ROS generated was also measured. HepG2 cells were seeded in 24-well tissue culture plates at a density of 5×10^4 cells per well. After 24 h, the medium was removed, replaced by 0.1 mL tested sample and 0.9 mL medium, and cultured for 85 min. In each well, 0.5 mL of medium containing 10 μM 2′,7′-dichlorodihydrofluorescein diacetate (DCFH-DA, Sigma, USA) was added and reacted for 30 min, where the intracellular ROS turned the reagent to green fluorescent DCF. The reagent was then removed and wells were rinsed by the phosphate buffered saline (PBS). The fluorescence of trypsinized cells was measured at an excitation/emission wavelength of 488 nm/528 nm and normalized to blank.

A murine macrophage cell line (J774A.1) was used for evaluation of the immune response of AgNP/NSQ. The culture medium was high glucose DMEM (Gibco, USA) containing 1% PSA, 10% FBS, and 1.5 g L^{-1} sodium bicarbonate. Cells were seeded in 24-well tissue culture plates at a density of 5×10^4 cells per well. After 24 h, the medium was removed, replaced by 0.1 mL sample and 0.9 mL medium, and cultured for 6 or 12 hours. The average size of the trypsinized cells was determined using a particle counter (Multisizer 3, Beckman Coulter, USA). The proinflammatory gene expression was analyzed by reverse transcription-polymerase chain reaction (RT-PCR). The PCR conditions and primer sequences followed those described.[30] The semi-quantification of gene/β-actin ratios was performed by capillary electrophoresis (HDA-GT12TM system, eGENE, USA).

Escherichia coli (JM109) was used as the bacterial strain for the antimicrobial test. The testing protocols followed ASTM E 2315-03. The nutrient broth, nutrient agar, plate count agar, and buffer were prepared according to the Japan Industrial Standard (JIS) Z 2801. The bacteria cultured on nutrient agar were inoculated into the nutrient broth and grown overnight in a shaker incubator (110 rpm) at 35 °C. The suspension was diluted to 1×10^7 colony forming units (CFU)/mL. To each of the sterilized tubes were added 2 mL of bacterial suspension, 2 mL of sample solutions, and 16 mL of buffer. After incubation at 35 °C for 24 h, the solutions were diluted serially to the proper concentration and daubed to the agar dish for manual counting.

Physico-chemical characterizaton of the nanocomposites of PCU and AgNP/NSQ

For TEM examination, PCU-AgNP/NSQ nanocomposites were cast from 10 wt% solution on copper grids, dried at 60 °C for 72 h, and further dried under vacuum at 60 °C for 48 h. The specimens were then stained with 2 wt% phosphotungstic acid (Alfa Aesar, Great Britain) for 1 min and examined by TEM (JEM-1200 EX II, JEOL, Japan). Phosphotungstic acid reacts with the carbonyl group,[31] and therefore the carbonyl rich soft segment domains of PCU would stain dark and reveal the distribution of soft segment domains in the PCU matrix.

The tensile properties were measured using a universal testing instrument (HT-8504, Hung Ta Co., Taiwan) following the ASTM standard protocol (ASTMD638.10). The Young's modulus, 100% secant modulus, tensile strength, and elongation for the specimens (20 mm long and 4.85 mm wide) were obtained at a stretching rate of 100 mm min^{-1}.

The thermal properties of PCU-AgNP/NSQ were evaluated by TGA, with a heating rate of 10 °C per min from 100 to 750 °C. The onset temperature of pyrolysis (T_{onset}) and peak temperature of pyrolysis (T_p) were obtained from the TGA curves. The glass transition temperature (T_g) was determined from the second scan using a differential scanning calorimeter (DSC, Perkin Elmer Pyris 6, Perkin Elmer, USA), with a heating rate of 10 °C per min from −80 to 250 °C.

Small-angle X-ray scattering (SAXS) profiles of PCU-AgNP/NSQ were measured by a SAXS instrument at the beamline 23A1 of the National Synchrotron Radiation Research Center (Hsinchu, Taiwan). The photon energy was at about 8 keV. The range of scattering vector ($\boldsymbol{Q}$) was from zero to 0.155 ($Å^{-1}$).

Endothelial cell proliferation and macrophage activation on PCU-AgNP/NSQ

Bovine endothelial cells (ECs) were used for the test. The culture medium was low glucose DMEM containing 1% penicillin–streptomycin (Caissonlabs, USA), 10% FBS, and 1.7 g L^{-1} sodium bicarbonate. Thin films of PCU-AgNP/NSQ on a coverslip glass (15 mm diameter) were sterilized by 75% ethanol, rinsed with PBS for several times, and placed into the bottom of 24-well plates. Each well was seeded with 2×10^4 ECs. After 72 h, the medium was removed and washed by PBS for several times. The number of trypsinized cells was counted using a hemocytometer.

To evaluate the inflammatory response, macrophages (J774A.1) were seeded in 24-well tissue culture plates at a density of 5×10^4 per well. After 24 and 72 h, the medium was removed and washed by PBS for several times. Cells were collected and analyzed for the average size and proinflammatory gene expression as previously described. Cells seeded in a blank well (tissue culture polystyrene, TCPS) served as the control for each experiment.

Antimicrobial activities of PCU-AgNP/NSQ

The antimicrobial activities of PCU-AgNP/NSQ were evaluated by following the protocol of JIS Z 2801. Soybean-casein digest broth (BD Bioscience, USA) with lecithin polysorbate (MP Biomedicals, USA) (SCDLP) was prepared. Each sample (5×5 cm^2) was sterilized by 75% ethanol and rinsed by DDW for several times. The bacterial suspension was prepared and diluted to 2.5×10^5–1×10^6 CFU mL^{-1}. Each sample was inoculated with 0.4 mL of bacterial suspension and covered with a sterilized polyethylene film. After incubation at 35 °C for 24 h, the samples were placed into tubes with 10 mL SCDLP broth and shaken for 10 minutes. The suspensions were diluted serially for CFU counting. PCU specimens added to SCDLP immediately after inoculation (without incubation) served as the immediate control. The microbiostatic ratio (%) was calculated as follows: (CFU of the immediate control − CFU of samples)/CFU of the immediate control × 100%.

Biocompatibility of PCU-AgNP/NSQ *in vivo*

PCU-AgNP/NSQ thick films (1×1 cm^2, 0.2 mm thick) were sterilized by 75% ethanol and rinsed by PBS. All animal procedures in this study were approved by the Institutional Animal Care and Use Committee of the university. Adult male Sprague-Dawley rats (400–450 g) were anesthetized by isoflurane. Two incisions (1 cm × 1 cm) were created on each side of the dorsum with proper distance. Samples were inserted into each subcutaneous site in a random order. After 30 days, rats were euthanized by CO_2 overdose treatment and all samples were explanted. The samples were washed extensively in 1% Tween-20 (Gerbu, Germany) solution followed by DDW, and dried in a vacuum oven for surface examination using a field emission scanning electron microscope (FESEM, Hitachi S-4800, Japan). The surrounding tissue was cut and fixed in 10% neutral formalin solution, embedded in paraffin, thin-sectioned, and stained by H&E for histological analysis under an optical microscope. The average capsule thickness was analyzed from the images using Image-J software. The residual weight after implantation was expressed as percent initial weight (%) which was defined as: (weight of the films after implantation/weight of the films before implantation) × 100%.

Statistical analysis

Multiple samples were used in each experiment. Each experiment was repeated independently for at least two times to assure reproducibility. Data from a typical experiment were shown. All measured values were expressed as mean ± standard deviation and analyzed by Student's *t*-test to obtain the *p* value. The statistical significances between the experimental groups were defined as $p < 0.05$.

Results and discussion

Properties of AgNP/NSQ and PCU

The measured organic fraction of NSQ in the hybrid was 58.8 wt%, greater than the theoretical value (50 wt%). The measured silver content in the hybrid was 6.59 wt%, smaller than the theoretical value (7 wt%). The surface of NSP has plenty of sodium ions that may attract lone-pair rich surfactant molecules such as the PEO-based surfactant used in the current study, giving NSQ an organic fraction greater than the theoretical value. The residual silver ion and the free (detached) AgNPs each accounted for 0.76 wt% and 0.4 wt% in all silver. This indicated that a predominant amount (~98.84 wt%) of silver had been anchored on NSQ.

The TEM image of the nanohybrid is shown in Fig. 1A. AgNPs on the hybrid were 4–12 nm in diameter with a mean of 7.39 ± 1.87 nm. The hydrodynamic diameters and zeta potentials of the nanomaterials involved in this study are summarized in Table 1. The average hydrodynamic diameter of NSQ was 355.1 ± 54.6 nm, which was smaller than that of NSP (402.9 ± 57.9 nm). The hydrodynamic diameter of AgNP/NSQ (28.8 ± 8.8 nm) and AgNP/NSP (29.8 ± 10.7 nm) was much smaller than that of NSQ and NSP. For physically produced AgNPs, the hydrodynamic diameter and zeta potential were 39.6 ± 13.3 nm and 3.63 ± 0.35 mV, respectively. AgNP/NSQ, AgNP/NSP, NSQ, and NSP all had a negative zeta potential (−35 to −28 mV), suggesting that they were more stably dispersed in water than the physically produced AgNPs. The lower hydrodynamic diameter of NSQ relative to NSP may be caused by the steric hindrance of the surfactant that prevents NSP from self-assembly. On the other hand, the PEO-based surfactant with a long alkyl chain might interfere with the reduction of silver ion. This may explain why the measured silver content in AgNP/NSQ was lower than the theoretical one. Even so, AgNPs (~7 nm

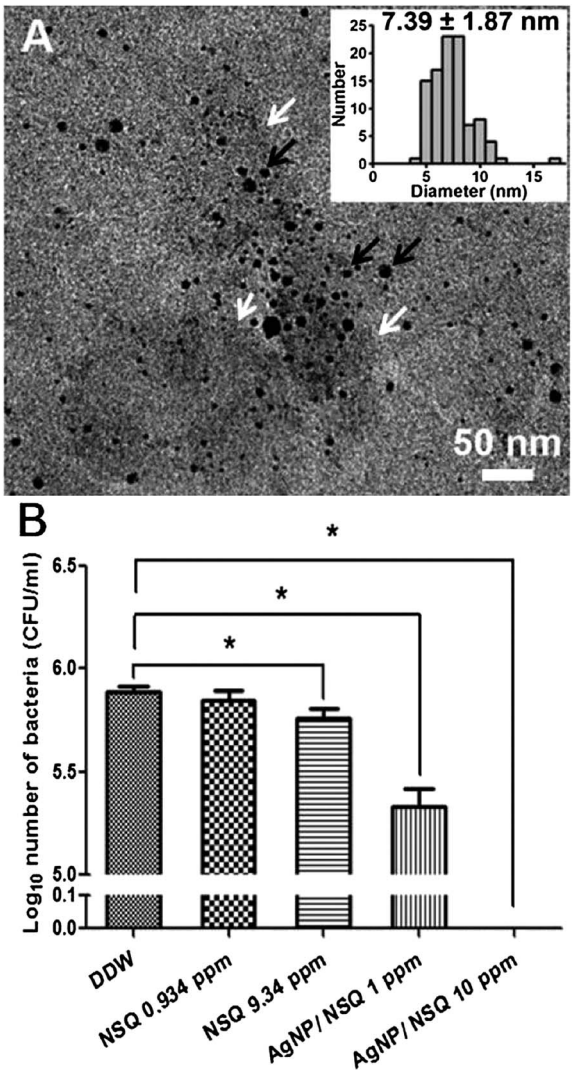

Fig. 1 (A) The typical TEM image of AgNP/NSQ with the size distribution shown in the right corner. The black and white arrows indicate AgNPs and NSP in the nanohybrid. (B) The antibacterial activities of AgNP/NSQ and NSQ against *E. coli*. * refers to $p < 0.05$.

Table 1 The average hydrodynamic diameter and zeta potential for different nanomaterials used in this study

Nanomaterials	Hydrodynamic diameter (nm)	Zeta potential (mV)
AgNP/NSQ	28.8 ± 8.8	−27.8 ± 0.4
AgNP/NSP	29.8 ± 10.7	−29.3 ± 0.3
NSQ	355.1 ± 54.6	−34.6 ± 0.3
NSP	402.9 ± 57.9	−34.3 ± 0.1
AgNPs	39.6 ± 13.3	3.63 ± 0.35

average) were successfully immobilized on NSQ and the purity of the nanohybrid was pretty high.

The antimicrobial activity of AgNP/NSQ is shown in Fig. 1B. AgNP/NSQ at a concentration of 10 ppm reduced the bacterial colonies remarkably (a 99.99% reduction), indicating that AgNP/NSQ had exhibited excellent bactericidal ability when the silver content was only 0.66 ppm. The antibacterial efficiency of AgNP/NSQ was even greater than AgNPs (Fig. S1, see ESI for all supplementary figures†). NSQ alone at the corresponding concentration did not show significant antibacterial effects. The physico-chemical properties of PCU synthesized in this study and those of Pellethane are summarized in Table 2. PCU could be successfully synthesized by the catalyst-free process. The average molecular weight increased as the molar ratio of the soft segment increased while the polydispersity remained in a moderate range (1.7–2.8). The molecular weight was in the order of: Pellethane > PCU651 > PCU431 > PCU541 > PCU321 > PCU211. The polydispersity was in the order of: PCU431 > PCU321 ≈ PCU211 > PCU651 > Pellethane > PCU541. PCU is generally regarded as biodurable PU and was used as the model polymer matrix for loading AgNP/NSQ in this study. The physico-chemical properties of the synthesized PCU were apparently varied by the stoichiometric ratios. Theoretically, when a higher ratio of MDI is used, there are more reactive sites for chain extension while the possibility of a random reaction between isocyanates and hydroxyl groups also increases. The side reaction of isocyanates also causes the termination of chain extension, leading to high polydispersity. A lower MDI ratio, on the other hand, provides fewer reactive sites but with less side reactions. Meanwhile, the stronger interaction between the oxygen and lone-pair rich soft segment may result in better thermal stability. Overall, a proper stoichiometric ratio should be considered for PCU synthesis.

Cytotoxicity and immune response of the AgNP/NSQ nanohybrid

The cytotoxicity of the AgNP/NSQ nanohybrid is shown in Fig. 2A for L929 cells and Fig. 2B for HepG2 cells. Both AgNP/NSQ and NSQ caused an obvious decrease in cell viability at a concentration of 50 ppm or beyond. To clarify which component in AgNP/NSQ caused cytotoxicity, a comparison of the cytotoxicity among AgNP/NSQ, AgNP/NSP, NSQ, NSP, and AgNPs is shown in Fig. S2.† AgNP/NSQ at 10 ppm caused a similar cytotoxic effect to L929 compared with AgNP/NSP (8.05 ppm) at the same silver level but without the surfactant. No significant cytotoxicity to L929 was observed for NSQ at 9.34 ppm or NSP at 3.736 ppm (which was the NSP fraction in 9.34 ppm NSQ). AgNP/NSP compared to AgNP/NSQ of the same silver level was more cytotoxic to HepG2. Moreover, NSQ at 9.34 ppm was less cytotoxic to HepG2 than NSP at 3.736 ppm. Physically manufactured AgNPs at 0.66 ppm, which had the same amount of silver as 10 ppm AgNP/NSQ, showed no significant cytotoxicity to HepG2. AgNP/NSQ showed a higher toxicity to L929, which may be associated with the additional presence of NSQ and the better dispersion of AgNPs as compared with the physically manufactured AgNPs. Overall, AgNP/NSQ, NSQ, and AgNP/NSP showed similar cytotoxic effects to L929, whereas to HepG2 the order of cytotoxicity was AgNP/NSP > AgNP/NSQ > NSQ. Cytotoxicity from the minor content of residual silver ion was not obvious (data not shown).

The *in situ* OCR and ECAR ratios for HepG2 cells exposed to different nanomaterials are demonstrated in Fig. 3A and B. Upon

Table 2 Sample abbreviation and monomer ratio for the poly(carbonate)urethanes (PCU) synthesized in this study and their physico-chemical properties[a]

Sample abbreviation	Molar ratio[b]	M_w	PDI[c]	Young's modulus (MPa)	100% Secant modulus (MPa)	Tensile strength (MPa)	Elongation (%)	T_{onset}[d] (°C)	T_p[e] (°C)	T_g[f] (°C)
Pellethane	—	182 043	1.9	15.6 ± 0.8	5.4 ± 0.4	34.6 ± 3.5	557 ± 38	n/a	n/a	n/a
PCU211	2 : 1 : 1	71 237	2.5	8.5 ± 0.8	1.2 ± 0.1	1.5 ± 0.1	596 ± 54	296.4	352.6	−23.0
PCU321	3 : 2 : 1	109 168	2.5	4.8 ± 0.6	0.8 ± 0.1	3.3 ± 0.8	1370 ± 159	293.0	345.9	−23.6
PCU431	4 : 3 : 1	147 924	2.8	2.9 ± 0.3	0.6 ± 0.1	2.0 ± 0.2	1360 ± 84	301.5	353.8	−24.4
PCU541	5 : 4 : 1	133 064	1.7	4.5 ± 0.3	0.9 ± 0.1	4.1 ± 0.5	1123 ± 105	301.2	357.9	−26.3
PCU651	6 : 5 : 1	154 897	2.4	4.1 ± 0.6	0.9 ± 0.0	5.2 ± 0.5	1177 ± 63	314.0	360.2	−27.4

[a] Pellethane was the commercially available poly(ether)urethane used for comparison. [b] MDI/macrodiol/chain extender. [c] Symbols: polydispersity. [d] Onset temperature of pyrolysis. [e] Peak temperature of pyrolysis. [f] Glass transition temperature.

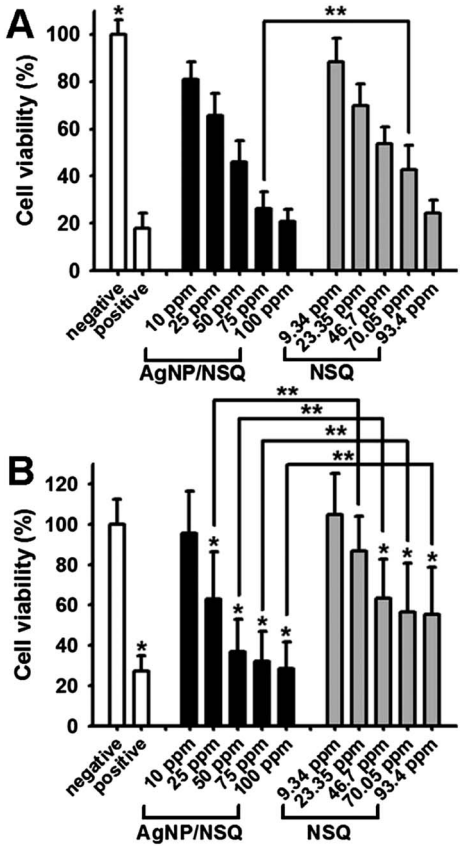

Fig. 2 Cytotoxicity of AgNP/NSQ and NSQ to (A) L929 fibroblasts and (B) HepG2 hepatocarcinoma cells. Significance ($p < 0.05$) in (A): * higher than all the other groups; in (B): * smaller than the negative control. ** Between the indicated groups. All ppm values are based on the weight of the nanomaterials, not the silver content.

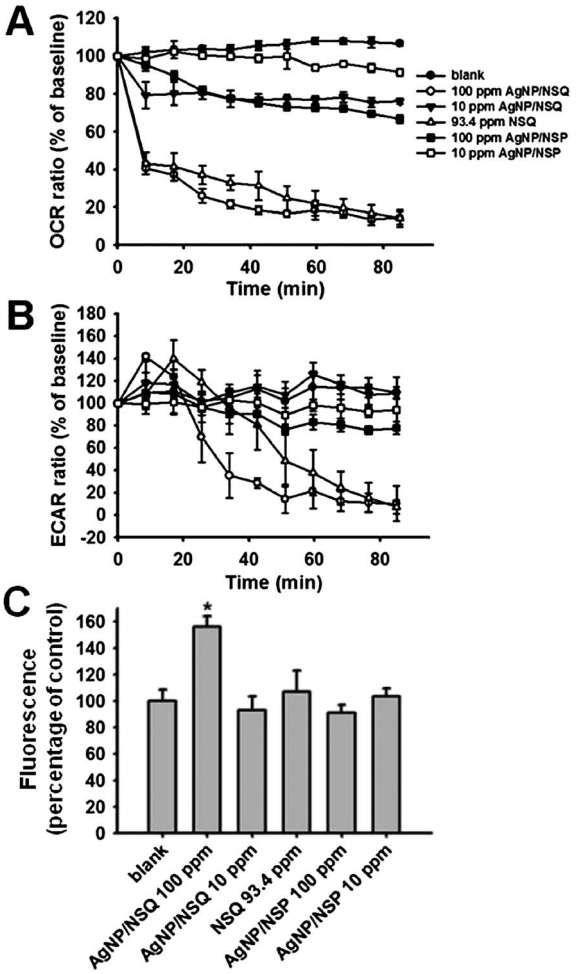

Fig. 3 (A) OCR ratio, (B) ECAR ratio, and (C) relative amount of ROS generated for HepG2 exposed to AgNP/NSQ, NSQ, or AgNP/NSP. OCAR and ECAR ratios were monitored by the XF extracellular flux analyzer for 85 min after exposure. The amount of ROS generated was measured for cells collected after 85 min of exposure and expressed as the fluorescence normalized to the blank. Significance ($p < 0.05$) in (C): * higher than all the other groups.

the exposure of 100 ppm AgNP/NSQ or 93.4 ppm NSQ, the OCR ratios obviously decreased while the ECAR ratios first increased and then decreased. No significant change occurred in the groups exposed to either AgNP/NSP or a lower concentration (10 ppm) of AgNP/NSQ. The intracellular ROS of HepG2 cells after exposure to the nanomaterials for 85 min is shown in Fig. 3C. AgNP/NSQ at 100 ppm stimulated more ROS generation than AgNP/NSP at 100 ppm or NSQ at 93.4 ppm. One of the functions of capping agents is the shielding effect that attenuates the direct exposure of nanomaterials to cells. The shielding effect from the surfactant was verified by the cytotoxicity test of HepG2 in this study, where NSQ was less cytotoxic than NSP alone. This effect was not as obvious in L929 fibroblasts. The shielding effect of the surfactant on HepG2 toxicity was still present in AgNP/NSQ *vs.* AgNP/NSP. Once the concentration of the nanomaterials increases, the shielding effect may be too weak to protect cells

from the toxicity of the nanomaterials. The cytotoxicity of the AgNP/NSQ nanohybrid seems to come from that of NSQ and the immobilized AgNPs, as free AgNPs at the corresponding concentration did not cause significant cytotoxicity. The OCR ratio represents the oxidative phosphorylation function and the ECAR ratio represents the glycolysis function. Once HepG2 cells were exposed to higher concentrations of AgNP/NSQ or NSQ, the activity of oxidative phosphorylation decreased. In the meantime, cells strived to compensate the insufficient adenosine triphosphate (ATP) by glycolysis but failed when the exposure time was prolonged. ROS might be the cause for the disturbed metabolic function exerted by AgNP/NSQ or NSQ. The direct intracellular ROS measurement, on the other hand, showed more ROS upon the exposure of AgNP/NSQ but not NSQ. The exact mechanism by which NSQ disturbed the cellular metabolic function is yet to be explored. Stimulation of ROS production may simultaneously account for the antimicrobial ability of AgNP/NSQ. Since AgNP/NSP did not disturb the early metabolic function as much as AgNP/NSQ, the more severe HepG2 cytotoxicity observed for AgNP/NSP *vs.* AgNP/NSQ may arise from other reasons.

The proinflammatory gene expression in macrophages exposed to 10 ppm AgNP/NSQ is shown in Fig. S3.† No significant increase in proinflammatory gene expression was observed when the exposure time was up to 12 h. At each time point, the proinflammatory gene expression in the AgNP/NSQ treated group was slightly lower than other treatment groups while NSQ alone appeared to provoke the highest gene expression. Judging from the expression profile, the immune response was likely to be NSQ > NSP > AgNP/NSP > AgNP/NSQ ≈ blank ≈ AgNPs. In particular, AgNP/NSQ at 10 ppm did not stimulate the proinflammatory gene expression of macrophages. AgNPs, especially in small sizes, may cause inflammatory reactions.[4] Wong *et al.*[32] showed that a small amount of AgNPs could reduce the immune response of J774A.1 macrophages without significant cytotoxicity. Therefore, AgNPs may be anti-inflammatory in certain conditions. This may explain the lower immune response of the nanohybrids (AgNP/NSQ as well as AgNP/NSP) compared to the carriers (NSQ or NSP). The surfactant shielding effect mentioned above was observed in AgNP/NSQ (*vs.* AgNP/NSP) but not in NSQ (*vs.* NSP). Specifically, AgNP/NSQ at 10 ppm did not stimulate macrophages, which is a rather promising finding.

Physico-chemical characterization of the nanocomposites of PCU and AgNP/NSQ

The mechanical and thermal properties of all synthesized PCU are included in Table 2. PCU211, compared to PCU651, had a higher Young's modulus and 100% secant modulus but lower tensile strength and elongation. As the proportion of the soft segment increased, the thermal stability represented by the pyrolytic temperature (T_{onset} or T_p) increased while the value of T_g decreased. An initial survey of the cell compatibility using ECs is shown in Fig. S4.† All PCU had similar cell attachment at 24 h. On PCU431 and PCU651, cells proliferated slightly faster and the cell number at 72 h was a little greater.

PCU211 and PCU651 were selected as the model polymers for making nanocomposites with AgNP/NSQ. The appearance of PCU would turn slightly yellowish after adding AgNP/NSQ, but the transparency did not change obviously (at the concentrations tested). TEM images for PCU-AgNP/NSQ nanocomposites are shown in Fig. 4. The stained soft segment of PCU was a little darker in the background while the exfoliated AgNP/NSQ with a clear edge was observed as the darkest spots dispersed in the soft segment domain. After adding AgNP/NSQ, the segregated soft segment domain present in the pristine PCU211 had transferred to a smaller worm-like structure distributed in the PCU matrix. Such a transition was not obvious in the system of PCU651. In PCU651-AgNP/NSQ containing more silver (*i.e.* 75 ppm), the soft segment domain became worm-like but the aggregated soft segment was still present.

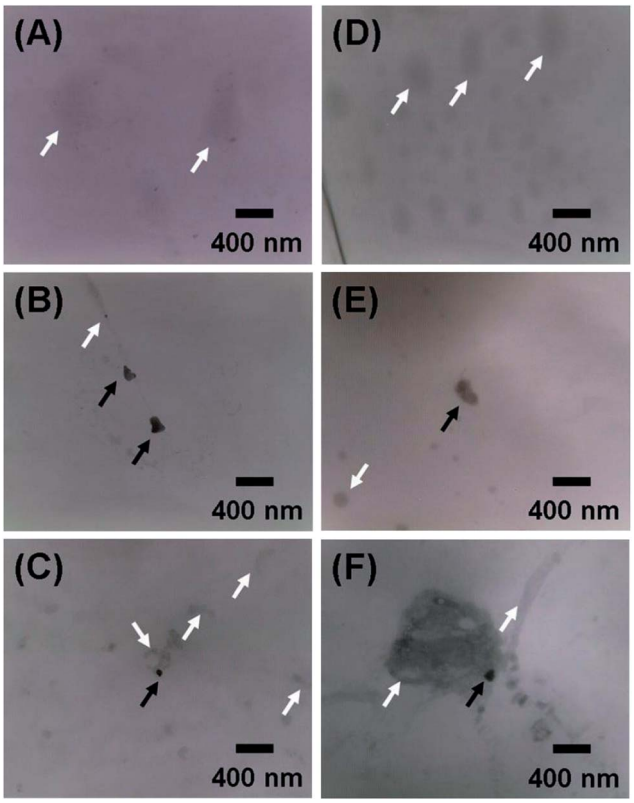

Fig. 4 TEM images for (A) PCU211, (B) PCU211-AgNP/NSQ 30, (C) PCU211-AgNP/NSQ 75, (D) PCU651, (E) PCU651-AgNP/NSQ 30, and (F) PCU651-AgNP/NSQ 75. The number 30 or 75 reflected the silver content (ppm) in the nanocomposite. All films on copper grids were stained by 2% phosphotungstic acid for 1 min before observation. The black and white arrows indicate the presence of AgNP/NSQ and segregated soft segment domains in the PCU matrix.

The tensile stress–strain curves of PCU211-AgNP/NSQ and PCU651-AgNP/NSQ nanocomposites are demonstrated in Fig. 5. The modulus, strength, and elongation are summarized in Table 3. Addition of AgNP/NSQ or NSQ produced a reinforcing effect on PCU211, where the stress–strain curve revealed a "strain-toughening" feature and the tensile strength was significantly increased by ten folds *vs.* the pristine PCU211 (Fig. 5A). Moreover, AgNP/NSQ more efficiently reinforced PCU211 than NSQ (Fig. 5B). In PCU651, loading AgNP/NSQ had no significant effect on the stress–strain behavior (Fig. 5C and D).

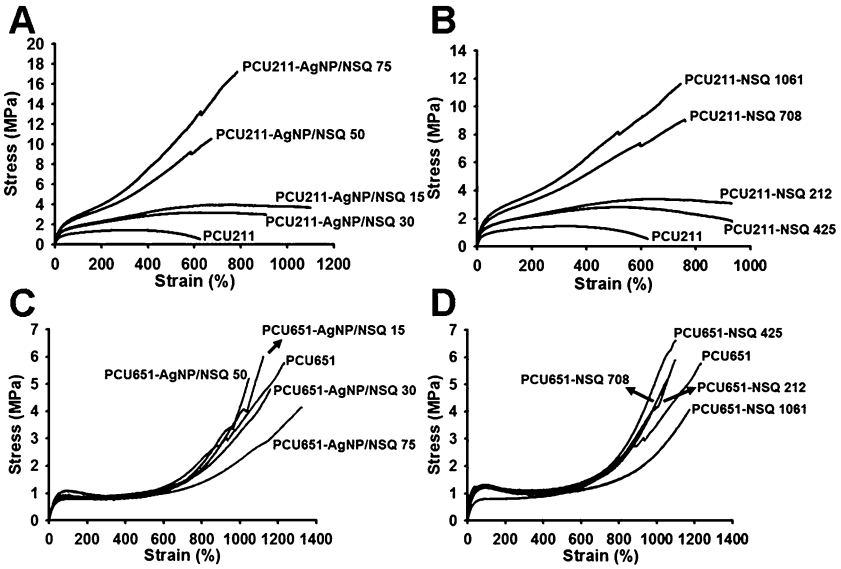

Fig. 5 Tensile stress–strain curves for (A) PCU211-AgNP/NSQ, (B) PCU211-NSQ, (C) PCU651-AgNP/NSQ, and (D) PCU651-NSQ nanocomposites.

Table 3 The physico-chemical properties of PCU211-AgNP/NSQ, PCU211-NSQ, PCU651-AgNP/NSQ, and PCU651-NSQ nanocomposites

Sample abbreviation	Young's modulus (MPa)	100% Secant modulus (MPa)	Tensile strength (MPa)	Elongation (%)	T_{onset} (°C)	T_p (°C)	T_g (°C)
PCU211	8.5 ± 0.8	1.2 ± 0.1	1.5 ± 0.1	596 ± 54	296.4	352.6	−23.0
PCU211-AgNP/NSQ 15[a]	11.2 ± 0.5	1.9 ± 0.1	3.9 ± 0.2	1019 ± 128	302.3	348.5	−23.5
PCU211-AgNP/NSQ 30	11.3 ± 1.4	1.8 ± 0.1	3.1 ± 0.4	908 ± 147	296.2	342.8	−23.6
PCU211-AgNP/NSQ 50	12.2 ± 0.9	2.5 ± 0.2	9.8 ± 2.6	646 ± 100	308.0	354.8	−25.0
PCU211-AgNP/NSQ 75	12.5 ± 0.7	2.9 ± 0.1	15.8 ± 1.0	762 ± 26	292.4	343.9	−28.0
PCU211-NSQ 212	11.4 ± 0.5	1.8 ± 0.1	3.3 ± 0.2	855 ± 148	296.1	350.2	−23.6
PCU211-NSQ 425	12.3 ± 1.1	1.8 ± 0.1	2.8 ± 0.1	937 ± 68	292.7	345.3	−24.8
PCU211-NSQ 708	12.9 ± 1.7	2.6 ± 0.2	9.1 ± 0.8	763 ± 44	286.1	343.3	−25.5
PCU211-NSQ 1061	12.7 ± 0.7	2.6 ± 0.2	10.3 ± 2.3	709 ± 114	291.6	347.5	−28.2
PCU651	4.1 ± 0.6	0.9 ± 0.0	5.2 ± 0.5	1177 ± 63	314.0	360.2	−27.4
PCU651-AgNP/NSQ 15	5.0 ± 0.9	1.3 ± 0.2	5.7 ± 0.7	1118 ± 45	321.8	370.8	−27.4
PCU651-AgNP/NSQ 30	3.2 ± 0.3	0.9 ± 0.1	4.8 ± 0.5	1159 ± 67	320.9	367.9	−29.3
PCU651-AgNP/NSQ 50	4.8 ± 1.0	1.3 ± 0.3	5.3 ± 0.8	1033 ± 56	317.5	367.8	−26.8
PCU651-AgNP/NSQ 75	4.1 ± 0.3	0.9 ± 0.0	4.0 ± 0.2	1276 ± 75	322.8	369.7	−26.2
PCU651-NSQ 212	4.8 ± 1.3	1.2 ± 0.3	5.4 ± 1.4	1051 ± 64	317.4	370.2	−25.8
PCU651-NSQ 425	5.6 ± 1.1	1.4 ± 0.2	7.0 ± 1.3	1109 ± 71	329.0	371.2	−26.4
PCU651-NSQ 708	4.0 ± 1.0	1.1 ± 0.3	4.4 ± 1.7	1029 ± 85	310.8	366.9	−25.8
PCU651-NSQ 1061	5.1 ± 2.0	1.0 ± 0.3	3.4 ± 0.6	1113 ± 44	323.8	371.3	−26.7

[a] The values are based on the silver content (ppm) in PCU-AgNP/NSQ nanocomposites. The content shown for NSQ in PCU-NSQ is the NSQ fraction equivalent to that in PCU-AgNP/NSQ (*e.g.* 212 ppm NSQ corresponding to the amount of NSQ in AgNP/NSQ with 15 ppm silver).

The thermal properties of the nanocomposites are also listed in Table 3. There was no significant change in the pyrolytic temperature when AgNP/NSQ was added to PCU211, while adding AgNP/NSQ to PCU651 improved the thermal stability. The addition of AgNP/NSQ decreased the value of T_g in the system of PCU211, but not in the system of PCU651. A lower T_g is often regarded as a greater degree of microphase separation in PU systems. The enhanced microphase separation by AgNP/NSQ seemed to support the mechanical reinforcement observed in PCU211 nanocomposites.

The SAXS profiles are shown in Fig. 6. The pristine PCU211 (Fig. 6A and B) showed a characteristic peak that shifted to lower q-ranges and eventually disappeared as the concentration of AgNP/NSQ increased. This observation indicated that the mean distance for the segregated hard domain may be greater for the PCU211-AgNP/NSQ nanocomposites. Nevertheless, such peak shifting was not observed in the system of PCU651 (Fig. 6C and D).

The mechanical property changes for PCU211 added with 0.12% of AgNP/NSQ or NSQ may result from changes in microstructures such as the degree of microphase separation. We therefore hypothesized that the hard segment in the pristine PCU211 may be aggregated, resulting in a lower degree of microphase separation and toughness. When AgNP/NSQ or NSQ was added, the surfactant may interact not only with the soft

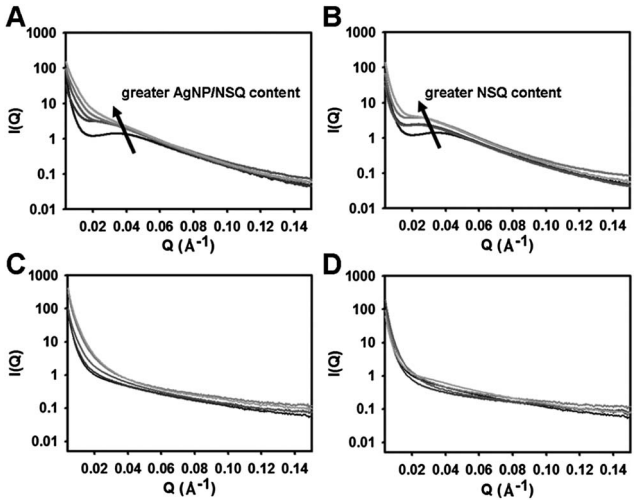

Fig. 6 SAXS profiles for (A) PCU211-AgNP/NSQ, (B) PCU211-NSQ, (C) PCU651-AgNP/NSQ, and (D) PCU651-NSQ nanocomposites. The darker line represents the nanocomposites with the smaller content of AgNP/NSQ or NSQ in the PCU matrix (refer to Table 3).

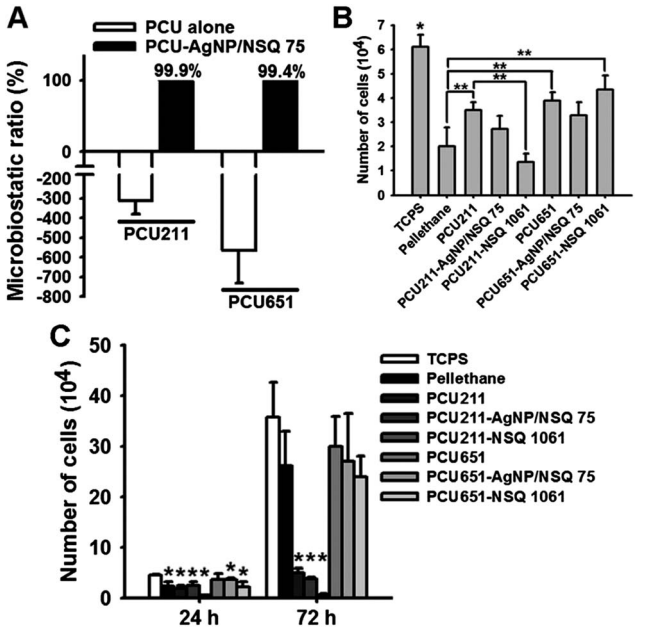

Fig. 7 (A) Microbiostatic ratios of PCU211-AgNP/NSQ and PCU651-AgNP/NSQ nanocomposites. All nanocomposites contain 75 ppm silver and 1061 ppm NSQ. (B) The number of ECs on PCU and the nanocomposites after incubation for 72 h. Significance ($p < 0.05$): * higher than all the other groups and ** between the indicated groups. (C) Attachment and proliferation of J774A.1 macrophages on PCU and the nanocomposites. Significance ($p < 0.05$): * lower than TCPS (tissue culture polystyrene).

segment but also with the hard segment, and hence improve the microphase separation and tensile properties. The immobilized AgNPs may further offer steric hindrance to prevent NSQ aggregation, making them more effective in regulating the microphase separation and reinforce PCU. We assumed that the above mechanisms may not exercise in the system with a lower hard segment ratio, *i.e.* PCU651. Similar trends of effects were revealed in SAXS profiles. SAXS is a useful technique for microstructure investigation of soft materials, *e.g.* the nano-scale alignment, shape, or the domain size of PU and its nanocomposite.[33] The characteristic peak in SAXS profiles presented earlier was likely to be the mean distance between the hard segment domains. Based on this assumption, AgNP/NSQ or NSQ may regulate the hard segment aggregation or microphase separation in the system of PCU211, as indicated by the increased mean distance of hard segment domains. This may also account for the improved tensile properties of PCU211 nanocomposites. The effect of AgNP/NSQ or NSQ on the mean distance of hard segment domains was not notable in the system of PCU651. Consistent with the tendency of the above observations, effects of AgNP/NSQ on cellular responses to the nanocomposites also seemed different for the two PCU systems. To assess the stability of AgNP/NSQ within the PCU matrix, we have performed extraction experiments for PCU-AgNP/NSQ. No silver in the extracts was detectable by inductively coupled plasma-mass spectrometry.

Antimicrobial activities of PCU-AgNP/NSQ

The microbiostatic ratios for PCU211-AgNP/NSQ and PCU651-AgNP/NSQ nanocomposites are shown in Fig. 7A. The microbiostasis was over 99% for both PCU-AgNP/NSQ nanocomposites containing 75 ppm silver, indicating remarkable antimicrobial effects. The microbiostatic ratios for the control PCU films were both negative, representing the continued growth of bacteria on the surface.

The PEO-based surfactant has a chemical structure similar to PC diol, which may account for the good dispersibility of AgNP/NSQ in the PCU matrix. The strong antimicrobial effect (~99% reduction) was retained in PCU-AgNP/NSQ nanocomposites though AgNP/NSQ seemed to be buried in the polymer matrix. It has been reported that cationic surfactant-capped NSP could float on the surface of Pellethane, resulting in good antimicrobial activity (~90% reduction) and biocompatibility.[29] Liu *et al.*[34] added bare AgNPs into waterborne PU and the nanocomposites containing 30 ppm AgNPs showed good antimicrobial activity (~94% reduction). Hsu *et al.*[35] considered that the dispersibility (non-aggregation) instead of the surface exposure of AgNPs in PU was critical for the antimicrobial activity. Basri *et al.*[36] employed polyvinylpyrrolidone to reduce silver nitrate in *N*-methylpyridine solution and form AgNPs in polyethersulfone. Since most AgNPs are not easily dispersed in polymers, the current AgNP/NSQ provides the possibility to blend small size AgNPs in a hydrophobic polymer without aggregation and therefore maximize the antimicrobial activity. Besides, AgNPs on NSQ keep their ability to further modulate the microstructure of PCU, as evident from SAXS findings.

Endothelial cell proliferation and macrophage activation on PCU-AgNP/NSQ

The number of ECs on PCU nanocomposites after incubation for 72 h is demonstrated in Fig. 7B. The effect of AgNP/NSQ or NSQ on EC proliferation during a period of 72 h was not evident except that a reduction was noticed for PCU211-NSQ. Pellethane

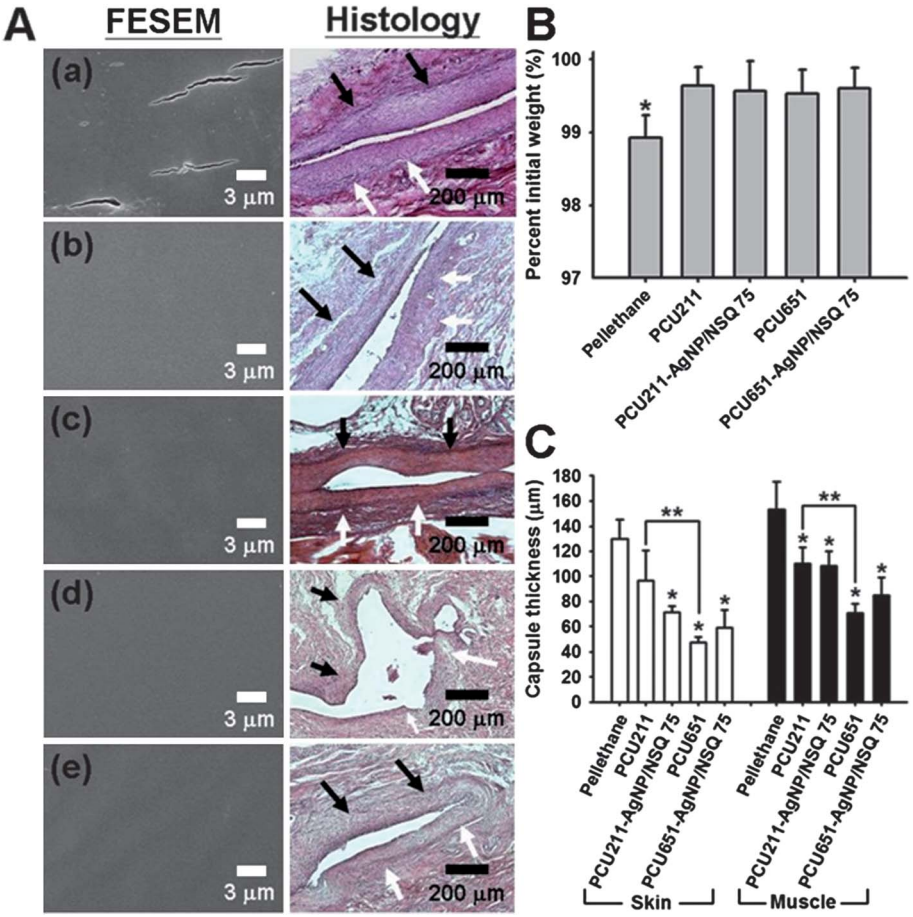

Fig. 8 (A) FESEM images for the surface of explanted films and histology of the foreign body capsule for (a) Pellethane, (b) PCU211, (c) PCU211-AgNP/NSQ 75, (d) PCU651, and (e) PCU651-AgNP/NSQ 75, after subcutaneous implantation in rats for 30 days. The black and white arrows indicate the muscle side and skin side of the capsules, respectively. (B) The residual weight after implantation, expressed as percent initial weight (%). Significance ($p < 0.05$): * lower than all the other groups. (C) The quantified capsule thickness for each material. Significance ($p < 0.05$): * lower than Pellethane and ** between the indicated groups.

showed fewer cells than the PCU series except for PCU211-NSQ. The proliferation of ECs on control (TCPS) was the greatest. The attachment and proliferation of J774A.1 macrophages on PCU nanocomposites are demonstrated in Fig. 7C. PCU211 and its nanocomposites had relatively fewer cells than the PCU651 series, Pellethane, and TCPS. On the other hand, the attachment and proliferation of macrophages on the PCU651 series and Pellethane were not significantly different from those on TCPS. The average size of macrophages is shown in Fig. S5A.† When the incubation time was prolonged (72 h), only the PCU211 series showed an increase in the macrophage size, suggesting a possible immune response. The proinflammatory gene expression of macrophages is shown in Fig. S5(B–D).† PCU211 provoked a higher level of IL-1 gene expression than PCU651 at 24 h. However, no significant difference was observed for the other proinflammatory genes at 24 h or 72 h.

Biocompatibility of PCU-AgNP/NSQ *in vivo*

The FESEM images of the nanocomposite films after 30 days implantation in rats are shown in Fig. 8A. No apparent surface degradation was observed in any of the PCU samples. Adding AgNP/NSQ in PCU did not influence the surface degradation. On the other hand, the surface of Pellethane showed several fissures, indicating degradation *in vivo*. The residual weight after the implantation is shown in Fig. 8B. Pellethane had the most weight loss among all groups. Histological images in Fig. 8A revealed the formation of foreign body capsules. The capsule thickness quantified from the images is displayed in Fig. 8C. The capsule thickness for Pellethane was greater than that for PCU or the nanocomposites at either the skin or muscle side. Pellethane is a commercial medical grade poly(ether urethane) (PEU) used in medical devices and healthcare products. A previous study indicated better *in vivo* biostability of PCUs *vs.* PEUs,[37] which was consistent with the current *in vivo* results. The biodurable PCU system shows favorable biocompatibility *in vitro* and *in vivo*, thus making PCU-AgNP/NSQ nanocomposites attractive antimicrobial materials for biomedical applications.

Conclusions

Fully delaminated montmorillonite NSP were organically modified by a neutral PEO-based surfactant and this surfactant-capped

NSP ("NSQ") was used to immobilize the silver nanoparticles (AgNPs) *via* the reduction of silver ion. The nanohybrid of AgNPs and NSQ (AgNP/NSQ) at a concentration of 10 ppm had a remarkable bactericidal effect as well as negligible cytotoxicity and proinflammatory response. The amphiphilic nanohybrid also provided a possibility to introduce antimicrobial AgNPs to the hydrophobic polymer matrix. Poly(carbonate)urethane (PCU) with different stoichiometric ratios of hard and soft segments was synthesized as a model polymer matrix for making AgNP/NSQ nanocomposites. The hard/soft segment ratio of PCU determined the effectiveness of AgNP/NSQ in modifying the microphase separation and physico-chemical properties of the polymer. Nanocomposites from PCU211 (MDI : macrodiol : chain extender ratio = 2 : 1 : 1) and AgNP/NSQ showed significant improvement in mechanical properties while those from PCU651 and AgNP/NSQ did not. PCU-AgNP/NSQ nanocomposites containing 75 ppm silver demonstrated outstanding antimicrobial ability, as well as better biodurability and biocompatibility than the commercial biomedical poly(ether)urethane. The nanohybrid of AgNP/NSQ thus offers the opportunity to prepare antimicrobial polymers for biomedical applications.

Acknowledgements

This research was supported by the National Research Program for Nanoscience and Technology sponsored by the National Science Council (101-2120-M-002-002). Technical support for the extracellular flux analyzer was kindly provided by Cell-Bio Biotechnology Co., Ltd.

References

1 C. N. Lok, C. M. Ho, R. Chen, Q. Y. He, W. Y. Yu, H. Z. Sun, P. K. H. Tam, J. F. Chiu and C. M. Che, *JBIC, J. Biol. Inorg. Chem.*, 2007, **12**, 527–534.
2 L. F. Espinosa-Cristobal, G. A. Matines-Castanon, R. E. Matinez-Martinez, J. P. Loyola-Rodriguez, N. Patino-Marin, J. F. Reyes-Macias and F. Ruiz, *Mater. Lett.*, 2009, **63**, 2603–2606.
3 P. V. AshaRani, G. L. K. Mun, M. P. Hande and S. Valiyaveettil, *ACS Nano*, 2009, **3**, 279–290.
4 M. V. D. Z. Park, A. M. Neigh, J. P. Vermeulen, L. J. J. de la Fonteyne, H. W. Verharen, J. J. Briede, H. van Loveren and W. H. de Jong, *Biomaterials*, 2011, **32**, 9810–9817.
5 F. Matinez-Gutierrez, E. P. Thi, J. M. Silverman, C. C. de Oliveira, S. L. Svensson, A. V. Hoek, E. M. Sanchez, N. E. Reiner, E. C. Gaynor, E. L. G. Pryzdial, E. M. Conway, E. Orrantia, F. Ruiz, Y. Av-Gay and H. Bach, *Nanomedicine: NBM*, 2011, **8**, 328–336.
6 C. A. Vaiana, M. K. Leonard, L. F. Drummy, K. M. Singh, A. Bubulya, R. A. Vaia, R. R. Naik and M. P. Kadakia, *Biomacromolecules*, 2011, **12**, 3139–3146.
7 R. X. Dong, C. C. Chou and J. J. Lin, *J. Mater. Chem.*, 2009, **19**, 2184–2188.
8 J. J. Lin, C. C. Chu, M. L. Chiang and W. C. Tsai, *J. Phys. Chem. B*, 2006, **110**, 18115–18120.
9 J. J. Lin, C. C. Chu, C. C. Chou and F. S. Shieu, *Adv. Mater.*, 2005, **17**, 301–304.
10 S. H. Hsu, H. J. Tseng, H. S. Hung, M. C. Wang, C. H. Hung, P. R. Li and J. J. Lin, *ACS Appl. Mater. Interfaces*, 2009, **1**, 2556–2564.
11 P. R. Li, J. C. Wei, Y. F. Chiu, H. L. Su, F. C. Peng and J. J. Lin, *ACS Appl. Mater. Interfaces*, 2010, **2**, 1608–1613.
12 H. L. Su, S. H. Lin, J. C. Wei, I. C. Pao, S. H. Chiao, C. C. Huang, S. Z. Lin and J. J. Lin, *PLoS One*, 2011, **6**, e21125.
13 R. S. Bezwada, in *Biomaterials*, ed. A. S. Kulshrestha, A. Mahapatro and L. A. Henderson, American Chemical Society, Washington, 2010, ch. 7, pp. 137–158.
14 J. V. Koleske, in *Encyclopedia of Materials: Science and Technology*, ed. K. H. J. Buschow, R. W. Cahn, M. C. Flemings, B. Ilschner, E. J. Kramer, S. Mahajan and P. Veyssiere, Elsevier, San Diego, 2001, p. 2472.
15 L. W. McKeen, in *The Effect of Creep and Other Time Related Factors on Plastics and Elastomers*, ed. L. W. McKeen, Elsevier, San Diego, 2nd edn, 2009, pp. 297–307.
16 L. W. McKeen, in *Fatigue and Tribological Properties of Plastics and Elastomers*, ed. L. W. McKeen, Elsevier, San Diego, 2nd edn, 2010, pp. 245–247.
17 P. A. Gunatillake and G. F. Meijs, in *Encyclopedia of Materials: Science and Technology*, ed. K. H. J. Buschow, R. W. Cahn, M. C. Flemings, B. Ilschner, E. J. Kramer, S. Mahajan and P. Veyssiere, Elsevier, San Diego, 2001, pp. 7746–7752.
18 Y. Marois and R. Guidoin, in *Biomedical Applications of Polyurethanes*, ed. P. Vermette, H. J. Griesser, G. Laroche and R. Guidoin, Landes Bioscience, Georgetown, 2001, p. 87.
19 F. Huang, Y. Marois, R. Roy, M. Julien and R. Guidoin, *Biomaterials*, 1992, **13**, 209–216.
20 S. H. Hsu and Y. C. Kao, *Macromol. Biosci.*, 2005, **5**, 246–253.
21 S. H. Hsu and Y. C. Kao, *Macromol. Biosci.*, 2004, **4**, 891–900.
22 S. H. Hsu, Y. C. Kao and Z. C. Lin, *Macromol. Biosci.*, 2004, **4**, 464–470.
23 M. C. Tanzi, D. Mantovani, P. Petrini, R. Guidoin and G. J. Laroche, *J. Biomed. Mater. Res., Part A*, 1997, **36**, 550–559.
24 E. M. Christenson, M. Dadsetan, M. Wiggins, J. M. Anderson and A. Hiltner, *J. Biomed. Mater. Res., Part A*, 2004, **69**, 407–416.
25 S. H. Hsu, C. M. Tang and H. J. Tseng, *Biomacromolecules*, 2008, **9**, 241–248.
26 R. L. Orefice, E. Ayres, M. M. Pereira and H. S. Mansur, *Macromolecules*, 2005, **38**, 4058–4060.
27 M. Song, H. S. Xia, K. J. Yao and D. J. Hourston, *Eur. Polym. J.*, 2005, **41**, 259–266.
28 J. J. Lin, C. C. Chu, M. L. Chiang and W. C. Tsai, *Adv. Mater.*, 2006, **18**, 3248–3252.
29 M. C. Wang, J. J. Lin, H. J. Tseng and S. H. Hsu, *ACS Appl. Mater. Interfaces*, 2012, **4**, 338–350.
30 H. J. Yen, S. H. Hsu and C. L. Tsai, *Small*, 2009, **5**, 1553–1561.
31 D. C. Pease, *J. Ultrastruct. Res.*, 1966, **15**, 555–588.

32 K. K. Y. Wong, S. O. F. Cheung, L. Huang, J. Niu, C. Tao, C. M. Ho, C. M. Che and P. K. H. Tam, *ChemMedChem*, 2009, **4**, 1129–1135.
33 Y. S. Sun, U. S. Jeng, Y. S. Huang, K. S. Liang, T. L. Lin and C. S. Tsao, *Physica B*, 2006, **385**, 650–652.
34 H. L. Liu, S. A. Dai, K. Y. Fu and S. H. Hsu, *Int. J. Nanomed.*, 2010, **5**, 1017–1028.
35 S. H. Hsu, H. J. Tseng and Y. C. Lin, *Biomaterials*, 2010, **31**, 6796–6808.
36 H. Basri, A. F. Ismail and M. Aziz, *Desalination*, 2011, **273**, 72–80.
37 E. M. Christenson, M. Dadsetan, J. M. Anderson and A. Hiltner, *J. Biomed. Mater. Res., Part A*, 2005, **74**, 141–155.